Critical dynamics of nonconserved N-vector models with anisotropic nonequilibrium perturbations

Sreedhar B. Dutta
School of Physics, Indian Institute of Science Education and Research, Thiruvananthapuram, India

Su-Chan Park (박수찬)*
Department of Physics, The Catholic University of Korea, Bucheon 420-743, Korea

(Received 18 November 2010; published 21 January 2011)

We study dynamic field theories for nonconserving N-vector models that are subject to spatial-anisotropic bias perturbations. We first investigate the conditions under which these field theories can have a single length scale. When $N = 2$ or $N \geqslant 4$, it turns out that there are no such field theories and, hence, the corresponding models are pushed by the bias into the Ising class. We further construct nontrivial field theories for the $N = 3$ case with certain bias perturbations and analyze the renormalization-group flow equations. We find that the three-component systems can exhibit rich critical behavior belonging to two different universality classes.

DOI: 10.1103/PhysRevE.83.011117 PACS number(s): 64.60.Ht, 05.40.−a, 05.70.Fh, 64.60.ae

I. INTRODUCTION

Classification of the universality exhibited by systems with macroscopic degrees of freedom, both at and away from equilibrium, is one of the main objectives that has been pursued in statistical physics ever since the advent of scaling theory and renormalization-group (RG) framework. The universality classes of nonequilibrium systems are far less understood, unlike those at equilibrium, in spite of having identified many nonequilibrium classes such as the absorbing phase transitions [1], growing surfaces [2], self-organized criticality [3], driven diffusive systems [4], and so on.

Constructing classes of infrared-stable field theories by taking a scaling limit of microscopic models is a formidable task, even at equilibrium. Hence, probing known field theories by various perturbations and following the induced instabilities, if any, is an alternative that can provide invaluable insights toward any classification.

Near-equilibrium critical dynamics is extensively studied and effectively captured by time-dependent Landau-Ginzburg (LG) models as categorized by Hohenberg and Halperin [5]. Recent studies have explored the effects of nonequilibrium perturbations on various dynamic universality classes [6–11]. They not only include perturbations about the LG energy functionals but also *genuine* nonequilibrium perturbations about the critical dynamics. The detailed-balance violating perturbations turn out to be relevant in the conserved systems [4,8,12]. On the other hand, it is well established that the kinetic Ising systems of Model-A class (in Hohenberg-Halperin classification) are stable against local dynamic perturbations, even if they violate detailed-balance conditions, provided that the symmetries are preserved [6,13]. Bassler and Schmittmann (BS) further found that the spatially anisotropic perturbations, in spite of not respecting the Z_2 symmetry, can not destabilize the dynamic class of nonconserved kinetic Ising models, which are described by a single-scalar order-parameter field [7]. This naturally brings forth the issue of whether the irrelevance of such spatially anisotropic perturbations pervades throughout Model-A systems or is only restricted to a subset, like those describable by a scalar order parameter. It was presumed that the N-component systems, such as kinetic Ising models, might also be robust to such perturbations [8,14]. We find that, upon investigating the role of spatially anistropic perturbations on N-component Model-A systems, this is not the case.

The structure of this paper is as follows: In Sec. II, we construct the N-component Model-A system with anisotropic nonequilibrium perturbations, and then address the possibility of constructing a field theory with a single characteristic length scale. We show that, unless $N = 3$, the system should belong to the Ising class, which is confirmed numerically for the case of $N = 2$. In Sec. III, we analyze $N = 3$ systems using the renormalization-group techniques. In Sec. IV, we summarize the results.

II. PERMUTATION-SYMMETRIC N-VECTOR DYNAMIC CRITICAL FIELD THEORIES

In this section, we construct nonconserving N-vector models subject to spatial-anisotropic perturbations and find the interactions consistent with a single length scale.

We consider the following class of N-vector models driven by a nonconserved Langevin dynamics:

$$\partial_t \phi_a(\boldsymbol{x},t) = \mathcal{F}_a(\phi(\boldsymbol{x},t)) + \eta_a(\boldsymbol{x},t), \tag{1}$$

with

$$\mathcal{F}_a(\phi) = (\nabla^2 - r)\phi_a + \frac{\mathcal{E}_{abc}}{2}\phi_b \partial_\parallel \phi_c - \frac{G_{abcd}}{3!}\phi_b\phi_c\phi_d, \tag{2}$$

where the indices a, b, c, and d run from 1 to N, the summation over repeated indices is assumed, and $\eta_a(\boldsymbol{x},t)$ denotes the Gaussian noise with zero mean and variance $\langle \eta_a(\boldsymbol{x},t)\eta_b(\boldsymbol{x}',t')\rangle = 2T\delta_{ab}\delta(\boldsymbol{x}-\boldsymbol{x}')\delta(t-t')$. Since $\phi_b\phi_c\phi_d = \phi_d\phi_b\phi_c$ and so on, we assume that, without any loss of generality, G_{abcd} is invariant under all permutations of $\{b,c,d\}$ ($G_{abcd} = G_{adbc}$, for example). The couplings $\mathcal{E}_{abc}$ introduce spatial anisotropy in the $x_\parallel$ direction. The spatial-anisotropic perturbations, often referred to as the bias, are straightforward generalizations of the bias perturbation in the BS model [7]. Note that the above G and $\mathcal{E}$ interaction terms are the most general marginal perturbations at $d = 4$.

It should be remarked that, if $\mathcal{F}_a(\phi)$ is derivable from a functional $S[\phi]$, namely, $\mathcal{F}_a(\phi)(\boldsymbol{x}) = -\delta S[\phi]/\delta\phi_a(\boldsymbol{x})$, then (under certain conditions) the system exhibits equilibrium

*spark0@catholic.ac.kr

behavior at large times. Any term that is not derivable from a functional when included will not allow the system to equilibrate; hence, it shall be referred to as *genuine* nonequilibrium perturbation. Unlike most of the G terms, the $\mathcal{E}$ terms are genuine nonequilibrium perturbations and can lead the system to a variety of nonequilibrium states.

We now investigate which of the interactions are consistent with a field theory with a single characteristic length scale in the long-time limit. We shall find such interactions by first demanding that the set of equations (1) are invariant under any permutation of the field components, and then demanding the existence of a single length scale.

A. Permutation-symmetric interactions

Let $\hat{P}$ be an operator transforming Langevin equations in such a way that $\hat{P}\partial_t\phi_a \equiv \partial_t\phi_{\mathcal{P}a}$ and

$$\begin{aligned}\hat{P}\mathcal{F}_a(\phi) &\equiv (\nabla^2 - r)\phi_{\mathcal{P}a} + \frac{1}{2}\sum_{bc}\mathcal{E}_{abc}\phi_{\mathcal{P}b}\partial_\parallel\phi_{\mathcal{P}c} \\ &\quad - \frac{1}{3!}\sum_{bcd}G_{abcd}\phi_{\mathcal{P}b}\phi_{\mathcal{P}c}\phi_{\mathcal{P}d} \\ &= (\nabla^2 - r)\phi_{\mathcal{P}a} + \frac{1}{2}\sum_{bc}\mathcal{E}_{a\mathcal{P}^{-1}b\mathcal{P}^{-1}c}\phi_b\partial_\parallel\phi_c \\ &\quad - \frac{1}{3!}\sum_{bcd}G_{a\mathcal{P}^{-1}b\mathcal{P}^{-1}c\mathcal{P}^{-1}d}\phi_b\phi_c\phi_d, \end{aligned} \tag{3}$$

where $\mathcal{P}$ is a permutation of field components $\{1,\ldots,N\} \mapsto \{\mathcal{P}1,\ldots,\mathcal{P}N\}$ with $\mathcal{P}^{-1}$ to be its inverse. Since a permutation-symmetric theory demands that Eq. (1) should be invariant under $\hat{P}$, that is, $\hat{P}\mathcal{F}_a = \mathcal{F}_{\mathcal{P}a}$, the coupling constants should satisfy $\mathcal{E}_{\mathcal{P}abc} = \mathcal{E}_{a\mathcal{P}^{-1}b\mathcal{P}^{-1}c}$ and $G_{\mathcal{P}abcd} = G_{a\mathcal{P}^{-1}b\mathcal{P}^{-1}c\mathcal{P}^{-1}d}$ or, equivalently,

$$\mathcal{E}_{abc} = \mathcal{E}_{\mathcal{P}a\mathcal{P}b\mathcal{P}c}, \quad G_{abcd} = G_{\mathcal{P}a\mathcal{P}b\mathcal{P}c\mathcal{P}d} \tag{4}$$

for all $\mathcal{P}$'s and a, b, c, and d.

The permutation symmetry in the dynamics will restrict the number of independent G couplings to seven, which are denoted as

$$G_{1111}, G_{1112}, G_{1122}, G_{1123}, G_{1222}, G_{1223}, G_{1234}. \tag{5}$$

The notation G_{1111} refers to those couplings G_{abcd}, where all the indices b, c, and d are the same as a, and G_{1112} is used when one of the indices b, c, and d is different from a, and so on. Recall that, by construction, G_{abcd} is assumed to be invariant under all permutations in $\{b,c,d\}$. If any of the indices of a coupling constant are greater than N, then that coupling constant is understood to be zero. Likewise, there are five allowed bias couplings:

$$\mathcal{E}_{111}, \mathcal{E}_{112}, \mathcal{E}_{121}, \mathcal{E}_{122}, \mathcal{E}_{123}. \tag{6}$$

Although the permutation symmetry does not require that $\mathcal{E}_{112} = \mathcal{E}_{121}$, it does demand that $\mathcal{E}_{123} = \mathcal{E}_{132}$.

Note that if we soften the permutation symmetry to cyclic-permutation symmetry, then there are a greater number of allowed coupling constants. We shall later consider dynamic models with only the cyclic-permutation symmetry.

B. Interactions consistent with a single length scale

In order to identify the couplings that are consistent with a single length scale (or mass scale), it is convenient to analyze Eq. (1) in Martin-Siggia-Rose (MSR) formalism [15]. The MSR action for Eq. (1) is given by

$$\begin{aligned}\mathcal{S}(\widetilde{\phi},\phi) &= \int_x [\widetilde{\phi}_a(\partial_t\phi_a - \mathcal{F}_a(\phi)) - T\widetilde{\phi}_a\widetilde{\phi}_a] \\ &= \int_x \Big[\widetilde{\phi}_a(\partial_t - \nabla^2 + r)\phi_a - \frac{1}{2}\mathcal{E}_{abc}\widetilde{\phi}_a\phi_b\partial_\parallel\phi_c \\ &\quad + \frac{1}{3!}G_{abcd}\widetilde{\phi}_a\phi_b\phi_c\phi_d - T\widetilde{\phi}_a\widetilde{\phi}_a\Big], \end{aligned} \tag{7}$$

where $\int_x \equiv \int dt d^d\boldsymbol{x}$, $\widetilde{\phi}_a$ refers to the auxiliary (response) field, the conventions $\phi_a = \phi_a(\boldsymbol{x},t)$ and $\widetilde{\phi}_a = \widetilde{\phi}_a(x,t)$ are used, and the summation over repeated indices is assumed.

The permutation symmetry in the above-constructed MSR action (7) with seven G couplings and five $\mathcal{E}$ couplings is only a necessary condition for a single length scale (or mass scale). However, it is not sufficient since there are other relevant terms allowed by the symmetry that may get generated during renormalization, such as $\widetilde{\phi}_a\widetilde{\phi}_b$, $\widetilde{\phi}_a\phi_b$, and $\widetilde{\phi}_a\partial_\parallel^2\phi_b$, where $a \neq b$. In particular, it is the off-diagonal mass term $\sum_{a\neq b}\widetilde{\phi}_a M_{ab}\phi_b$, if generated, that will introduce an extra length scale. In fact, the permutation symmetry will imply that all the diagonal elements are equal and, similarly, all the off-diagonal elements are equal. This mass matrix will have two eigenvalues, one of which is $N-1$ degenerate. Therefore, the presence of off-diagonal mass terms in an N-vector model indicates a crossover of the critical behavior to either that of a scalar model or to that of a $(N-1)$-vector model (which itself may not have a single length scale).

Now the question boils down to which form of the interactions will avoid the generation of the off-diagonal mass during renormalization. Before we present more general symmetry arguments for identifying those interactions, we shall specify the conditions that are imposed by perturbative corrections to second order.

At one loop, the $\mathcal{E}$ couplings may generate off-diagonal kinetic terms $\widetilde{\phi}_a\partial_\parallel^2\phi_b$, and the G couplings may generate off-diagonal mass terms proportional to $\sum_c G_{abcc}\widetilde{\phi}_a\phi_b$. The off-diagonal mass terms are absent only if the coupling constants satisfy the trace condition [16]: $\sum_c G_{abcc} = 0$ for $a \neq b$ and $N \geqslant 2$, which, when expressed explicitly, is

$$G_{1112} + G_{1222} + (N-2)G_{1223} = 0. \tag{8}$$

Provided the $\mathcal{E}$ couplings have generated nonzero off-diagonal kinetic terms at one loop, then the two-loop corrections to the off-diagonal mass are proportional to $\sum_{c,d} G_{abcd}\widetilde{\phi}_a\phi_b$. Hence, for the absence of off-diagonal mass terms, the coupling constants need to satisfy a further trace condition

$$\begin{aligned}&2G_{1122} + 2(N-2)(G_{1123} + G_{1223}) \\ &\quad + (N-2)(N-3)G_{1234} = 0. \end{aligned} \tag{9}$$

Finding further constraints from higher-order correction is rather cumbersome. Instead, we invoke symmetry arguments to find the coupling constants that are consistent with a single length scale. To this end, we define certain parity symmetries

and then explain how these symmetries can distinguish the presence or absence of off-diagonal mass. To any finite order, the effective action will contain terms of the form $(\tilde{n}_a, n_a \geqslant 0)$

$$\prod_{a=1}^{N} (\widetilde{\phi}_a)^{\tilde{n}_a} (\phi_a)^{n_a}, \tag{10}$$

suppressing the possible derivatives. If $(n_a + \tilde{n}_a) - (n_b + \tilde{n}_b)$ is even for any pair of a,b, we will define this term as parity symmetric. If a term is parity symmetric and, further, $n_1 + \tilde{n}_1$ is even (odd), this term is said to be even (odd) parity symmetric. Note that diagonal mass terms are even parity symmetric and off-diagonal mass terms are not parity symmetric unless $N = 2$, in which case they are odd parity symmetric. Essentially, the diagonal mass terms have different symmetry from the off-diagonal mass terms. In the case of $N > 2$, if the (bare) action contains interaction terms that are not parity symmetric, then the off-diagonal mass terms should emerge during renormalization; in the case $N = 2$, the odd parity symmetric interactions will also generate off-diagonal mass terms during renormalization.

It is easy to check that, for arbitrary N, the terms associated with G_{1111} and G_{1122} are even parity symmetric, while those combined with G_{1123} and G_{1223} are not parity symmetric. The couplings G_{1112} and G_{1222} generate terms that are not parity symmetric for $N > 2$, while they generate odd parity symmetric terms including off-diagonal mass for $N = 2$. Hence, the presence of any of the four couplings G_{1123}, G_{1223}, G_{1112}, and G_{1222} will generate off-diagonal mass terms, and these terms should be dropped in order to construct a field theory with a single length scale. The coupling G_{1234} is odd parity symmetric for $N = 4$, while it will generate terms that are not parity symmetric for $N > 4$. Hence, G_{1234} introduces off-diagonal mass for any $N > 4$, but not for $N = 4$. We shall not pursue further the $N = 4$ case because it is not relevant for the effects of spatial anisotropy,

Similarly, in multicomponent models with bias, the couplings $\mathcal{E}_{111}$, $\mathcal{E}_{112}$, $\mathcal{E}_{121}$, and $\mathcal{E}_{122}$ are not parity symmetric. The coupling constant $\mathcal{E}_{123}$ is not parity symmetric for $N > 3$, but it becomes odd parity symmetric for $N = 3$. Since the off-diagonal mass terms are not parity symmetric for $N = 3$, the symmetry embedded in $\mathcal{E}_{123}$ for $N = 3$ does not allow for the generation of off-diagonal mass during renormalization. Hence, $\mathcal{E}_{123}$ is the only coupling constant that does not generate off-diagonal mass, that too, only when $N = 3$. We summarize these results in Table I.

TABLE I. Parity of terms associated with each coupling constant. N-PS refers to not parity symmetric and E-PS and O-PS refer to even parity symmetric and odd parity symmetric, respectively.

N	N-PS	E-PS	O-PS
Any N	G_{1123}, G_{1223}	G_{1111}, G_{1122}	
$N = 2$			G_{1112}, G_{1222}
$N > 2$	G_{1112}, G_{1222}		
$N = 4$			G_{1234}
$N > 4$	G_{1234}		
$N > 1$	$\mathcal{E}_{111}, \mathcal{E}_{112}, , \mathcal{E}_{121}, \mathcal{E}_{122}$		
$N = 3$			$\mathcal{E}_{123}$
$N > 3$	$\mathcal{E}_{123}$		

TABLE II. Allowed multicomponent permutation-symmetric N-vector field theories with a single length scale.

Components	Allowed couplings
$N = 3$	$G_{1111}, G_{1122}, \mathcal{E}_{123}$
$N = 4$	$G_{1111}, G_{1122}, G_{1234}$
$N = 2$ or $N > 4$	G_{1111}, G_{1122}

Notice that the off-diagonal mass terms and the off-diagonal kinetic terms have the same parity symmetry. Therefore, the coupling constants that do not generate off-diagonal mass will also not generate off-diagonal kinetic terms, and, hence, the second trace condition is not applicable. As expected, all the field theories with a single length scale satisfy the first trace condition.

To summarize, as shown in Table II, we find that, for $N = 2$ or $N \geqslant 4$, the only N-vector field theories with a single length scale are those that do not have any coupling constants other than G_{1111} and G_{1122}. In these cases, the bias perturbations will eventually make the system cross over to the single-scalar field theory with bias that is studied in Ref. [7]. In the case of $N = 4$, the possible single-length-scale theories do not have any coupling constants other than G_{1111}, G_{1122}, and G_{1234}. Only in the case of $N = 3$ is it possible to have a single length-scale model subjected to bias, where the allowed coupling constants are G_{1111}, G_{1122}, and $\mathcal{E}_{123}$.

C. Numerical study for $N = 2$ with bias

In this section, we numerically confirm that an $N = 2$ model with bias crosses over to the Ising class.

Consider an $O(2)$-symmetric model on a two-dimensional lattice described by the Hamiltonian

$$\mathcal{H} = -\sum_{\langle n,m \rangle} \vec{\phi}_n \cdot \vec{\phi}_m + \sum_n \left(\frac{r + 2d}{2} \phi_n^2 + \frac{u}{4} \left(\phi_n^2\right)^2 \right), \tag{11}$$

where n is the site index, $\langle n,m \rangle$ denotes the sum over all nearest-neighbor pairs, $\vec{\phi}_n = (\phi_{n,1}, \phi_{n,2})$ is a real two-component vector field, and $\phi_n^2 := \vec{\phi}_n \cdot \vec{\phi}_n$. The dynamics of the field $\phi_{n,a}$ in the presence of a bias is governed by the following Langevin equation:

$$\frac{\partial}{\partial t} \phi_{n,a} = -\frac{\partial \mathcal{H}}{\partial \phi_{n,a}} + E \partial_{\parallel} \left(\phi_{n,a}^2\right) + \eta_{n,a}(t), \tag{12}$$

where $\eta_{n,a}$ is the white noise with correlation $\langle \eta_{n,a}(t) \eta_{n',a'}(t') \rangle = \delta_{nn'} \delta_{aa'} \delta(t - t')$ and $\partial_{\parallel}(\phi_{n,a}^2) := \phi_{n+1,a}^2 - \phi_{n-1,a}^2$, where $n + 1$ and $n - 1$ refer to the two nearest neighbors of n along a specified direction. In the absence of the bias $E = 0$, the steady state of Eq. (12) is described by the partition function

$$Z = \int_{-\infty}^{\infty} \left(\prod_n \prod_{a=1}^{2} d\phi_{n,a} \right) e^{-2\mathcal{H}}. \tag{13}$$

We have taken the two-dimensional square lattice to be of size $L \times L$ with periodic boundary conditions. The values of u and the bias E are set to unity, i.e., $u = E = 1$. Equation (12) is then integrated numerically by employing the Euler method with $\Delta t = 0.0025$. The initial condition is taken to be $\phi_{n,a} = \delta_{a,1}$ for all realizations. The system sizes of $L = 2^6$, 2^7, and 2^8

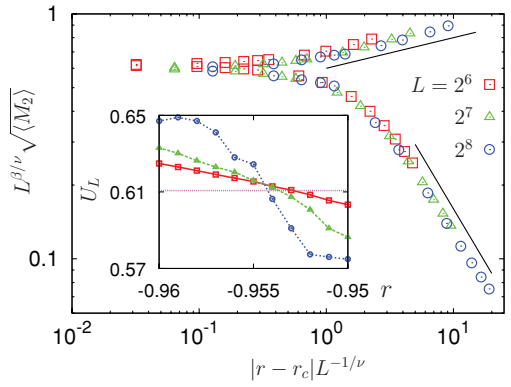

FIG. 1. (Color online) Finite-size scaling collapse using data for $L = 2^6$ (square), 2^7 (triangle), and 2^8 (circle). The upper (lower) straight line, the slope of which is $\frac{1}{8}$ $(-\frac{7}{8})$, indicates the expected asymptotic behavior of the scaling function up to a multiplication factor. Inset: Binder cumulants as a function of r for different system sizes as in the main figure. For comparison, the critical Binder cumulant for the Ising class is drawn as a straight line.

are considered, and the equilibration time is set to 20 000. After equilibration, we measured the magnetization $\vec{\mathcal{M}} = \sum_n(\phi_{n,1},\phi_{n,2})/L^2$ as well as $M_2 := |\vec{\mathcal{M}}|^2$ and $M_4 := M_2^2$ at every five unit times, namely, after every 2000 iterations with the above-mentioned Δt, and then obtained the averages for all these quantities. The critical point r_c is located using the Binder cumulant

$$U_L = 1 - \frac{\langle M_4\rangle}{3\langle M_2\rangle^2}. \tag{14}$$

The critical exponents β and ν are found from finite-size scaling by taking the scaling form for $\sqrt{\langle M_2\rangle}$ to be

$$\sqrt{\langle M_2\rangle} = L^{-\beta/\nu} f[(r_c - r)L^{1/\nu}]. \tag{15}$$

The asymptotic behavior of the universal scaling function f is given by

$$f(y) \to \begin{cases} y^{\beta} & \text{as } y \to \infty, \\ (-y)^{\beta-\nu} & \text{as } y \to -\infty. \end{cases} \tag{16}$$

Numerical results are shown in Fig. 1. The data collapse with the asymptotic behavior Eq. (16) are in good agreement with the critical exponents of the two-dimensional Ising model $\beta = \frac{1}{8}$ and $\nu = 1$ [18]. The critical point is located at $r_c = -0.9545 \pm 0.0010$, as shown in the inset of Fig. 1. The value of the critical cumulant is also consistent with that of the Ising model on a square lattice ($\simeq 0.6107$) [19]. Thus, the model with dynamics [Eq. (12)] clearly shows the order-disorder phase transition and exhibits critical behavior unlike its equilibrium counterpart, which can not undergo such a transition in two dimensions [20].

III. RENORMALIZATION-GROUP ANALYSIS OF $N = 3$ DYNAMIC FIELD THEORIES WITH CYCLIC-PERMUTATION SYMMETRY

In Sec. II B, we looked for permutation-symmetric N-vector field theories with a single length scale. Relaxing the symmetry to *cyclic-permutation* symmetry can lead us to a larger set of such field theories. In this section, we shall explore the renormalization-group fixed points of this larger set of dynamic field theories in the case $N = 3$.

By cyclic-permutation symmetry for $N = 3$, we mean the invariance of the MSR action under the transformation $\mathcal{CP} : 1 \to 2 \to 3 \to 1$. Note that $\mathcal{CP}$ symmetry distinguishes G_{1122} from G_{1133}, and furthermore allows us to include the term $(\phi_{a+2}\partial_\parallel\phi_{a+1} - \phi_{a+1}\partial_\parallel\phi_{a+2})$ in $\mathcal{F}_a(\phi)$. Hence, the MSR action for the $N = 3$ dynamic theory with $\mathcal{CP}$ symmetry can be written as

$$\begin{aligned} S = \sum_{a=1}^{3}\int_x \Big(&\widetilde{\phi}_a[\partial_t - D(\nabla_\perp^2 + \rho\partial_\parallel^2 - r)]\phi_a - T\widetilde{\phi}_a^2 \\ &+ \sum_{i=0}^{2}\frac{u_i}{3!}(3 - 2\delta_{i0})\widetilde{\phi}_a\phi_a\phi_{a+i}^2 + e_p\phi_{a+1}\phi_{a+2}\partial_\parallel\widetilde{\phi}_a \\ &+ e_m\widetilde{\phi}_a(\phi_{a+2}\partial_\parallel\phi_{a+1} - \phi_{a+1}\partial_\parallel\phi_{a+2})\Big). \end{aligned} \tag{17}$$

Here D and ρ are introduced, anticipating that these coupling constants flow separately under the RG. The field indices take modulo-3 integer values, and, hence, ϕ_4 and ϕ_5 mean ϕ_1 and ϕ_2, respectively. For notational simplicity, we relabel the couplings as $u_0 = G_{1111}$, $u_1 = G_{1122}$, $u_2 = G_{1133}$, and $e_p = \mathcal{E}_{123}$.

If we choose $u_1 = u_2$ and $e_m = 0$, then the action has full permutation symmetry, as discussed in Sec. II; for the choice $u_1 = u_2 = u_0/3$ and $e_m = e_p = 0$, it has $O(3)$ symmetry. A special case, with the choice $u_1 = u_2$ and $e_p = 0$, was studied in Ref. [11].

The free theory action is given by

$$S_0 = \sum_{a=1}^{3}\int_q \widetilde{\varphi}_a(-q)[-i\omega t + M(\boldsymbol{q})]\varphi_a(q), \tag{18}$$

where the φ are the Fourier-transformed fields

$$\widetilde{\phi}_a(\boldsymbol{x},t) = \int_q \exp(-i\omega t + i\boldsymbol{q}\cdot\boldsymbol{x})\widetilde{\varphi}_a(q), \tag{19}$$

$$\phi_a(\boldsymbol{x},t) = \int_q \exp(-i\omega t + i\boldsymbol{q}\cdot\boldsymbol{x})\varphi_a(q), \tag{20}$$

and q stands for the four-momentum $(\boldsymbol{q},\omega)$; the integral $\int_q := (2\pi)^{-(d+1)}\int d\omega d^d\boldsymbol{q}$; and

$$M(\boldsymbol{q}) = D(\boldsymbol{q}_\perp^2 + \rho q_\parallel^2 + r), \tag{21}$$

where $q_\parallel$ ($\boldsymbol{q}_\perp$) denotes the component of $\boldsymbol{q}$ parallel (perpendicular) to the bias direction. The free propagator is calculated as

$$\langle\tilde{\varphi}_a(q')\varphi_b(q)\rangle_0 = \frac{\delta_{ab}\bar{\delta}(q + q')}{-i\omega + M(\boldsymbol{q})} \equiv G_0(q)\delta_{ab}\bar{\delta}(q + q'), \tag{22}$$

where $\langle\cdots\rangle_0$ stands for the average over noninteracting theory (18), and the delta function $\bar{\delta}(q + q') := (2\pi)^{d+1}\delta(\omega + \omega')\delta(\boldsymbol{q} + \boldsymbol{q}')$. Graphical representation of the propagator and the interaction terms of the action (17) are shown in Fig. 2.

The generating functional of the correlation functions is

$$Z[J,\widetilde{J}] = \int \mathcal{D}\widetilde{\phi}\,\mathcal{D}\phi \exp\left(-S + \int_x \widetilde{J}\cdot\widetilde{\phi} + J\cdot\phi\right), \tag{23}$$

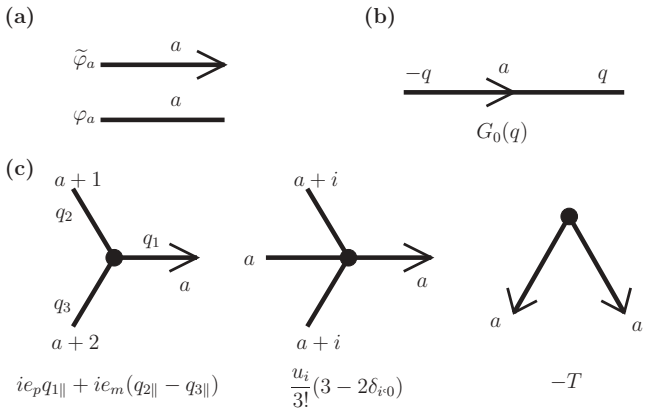

FIG. 2. Building blocks of the diagrammatic perturbations. (a) The field with (without) a tilde in the frequency-momentum domain is represented by a line segment with (without) an arrow head. (b) The propagator $G_0(q)$ is drawn using an arrow head in the middle. The four momentum of the field $\widetilde{\varphi}_a$ (φ_a) is $-q$ (q). (c) Three-, four-, and two-leg vertices are depicted with their interaction strength. The a can be any of {1,2,3} and $i \in \{0,1,2\}$.

where $J \cdot \phi = \sum_a J_a \phi_a$ and $\widetilde{J} \cdot \widetilde{\phi} = \sum_a \widetilde{J}_a \widetilde{\phi}_a$. The cumulants can be calculated by functional derivative of $F[\widetilde{J}, J] = \ln Z[\widetilde{J}, J]$ with respect to the sources such that

$$\begin{aligned} &G_{\tilde{n},n}(q_1,\ldots,q_{\tilde{n}};p_1,\ldots,p_n) \\ &= \left\langle \prod_{i=1}^{\tilde{n}} \widetilde{\varphi}_{a_i}(q_i) \prod_{k=1}^{n} \widetilde{\varphi}_{b_k}(p_k) \right\rangle_c \\ &= \prod_{i=1}^{\tilde{n}} \frac{\delta}{\delta \tilde{j}_{a_i}(-q_i)} \prod_{k=1}^{n} \frac{\delta}{\delta j_{b_k}(-p_k)} F[\tilde{j}, j] \Big|_{\tilde{j}=j=0}, \end{aligned} \quad (24)$$

where $\tilde{j}$ and j are the Fourier transformation of $\tilde{J}$ and J, respectively, and the multiplication factor $(2\pi)^{d+1}$ is assumed in the functional derivative with respective to j or $\tilde{j}$. This convention will also be used in Eq. (26). For convenience, the field indices are not written explicitly in $G_{\tilde{n},n}$. The vertex functions $\Gamma_{\tilde{m},m}$ can be obtained from $G_{\tilde{n},n}$ by a Legendre transformation

$$\Gamma[\widetilde{\psi}, \psi] = -F + \int_q [\tilde{j}(-q) \cdot \widetilde{\psi}(q) + j(-q) \cdot \psi(q)], \quad (25)$$

where

$$\widetilde{\psi}_a(q) = \frac{\delta F}{\delta \tilde{j}_a(-q)}, \quad \psi_a(q) = \frac{\delta F}{\delta j_a(-q)}. \quad (26)$$

The fields are written in terms of renormalized fields as

$$\widetilde{\phi}_a = Z_{\tilde{\phi}}^{1/2} \widetilde{\phi}_{aR}, \quad \phi_a = Z_\phi^{1/2} \phi_{aR}, \quad Z \equiv \sqrt{Z_{\tilde{\phi}} Z_\phi}, \quad (27)$$

and the parameters in terms of renormalized parameters as

$$\begin{aligned} D &= \frac{Z_D}{Z} D_R, \quad \rho = \frac{Z_\rho}{Z_D} \rho_R, \quad r = \frac{Z_r}{Z_D} r_R \mu^2, \\ u_0 &= \frac{Z_0}{Z Z_\phi} u_{0R}, \quad u_1 = \frac{Z_1}{Z Z_\phi} u_{1R}, \quad u_2 = \frac{Z_2}{Z Z_\phi} u_{2R}, \\ T &= \frac{Z_T}{Z_{\tilde{\phi}}} T_R, \quad e_p = \frac{Z_p}{Z Z_\phi^{1/2}} e_{pR}, \quad e_m = \frac{Z_m}{Z Z_\phi^{1/2}} e_{mR}, \end{aligned} \quad (28)$$

where R in the subscripts stands for the renormalized quantities and μ is an arbitrary momentum scale. Substituting these parameters in $\Gamma[\widetilde{\psi}, \psi]$ gives the generator $\Gamma_R[\widetilde{\psi}, \psi]$ of the renormalized vertex functions:

$$\begin{aligned} &\Gamma_{\tilde{m},m}^{a_1,\ldots,a_{m+\tilde{m}}}(\{q_i\}) \\ &= \prod_{i=1}^{\tilde{m}} \frac{\delta}{\delta \widetilde{\psi}_{a_i}(-q_i)} \prod_{j=\tilde{m}+1}^{\tilde{m}+m} \frac{\delta}{\delta \psi_{a_j}(-q_j)} \Gamma_R[\widetilde{\psi}, \psi] \Big|_{\widetilde{\psi}=\psi=0}. \end{aligned} \quad (29)$$

The renormalization factors are determined by the following set of normalization conditions:

$$\begin{aligned} &\Gamma_{1,1}^{11}(0;0) = r_R \mu^2, \quad \Gamma_{2,0}^{11}(q=0) = -2T_R, \quad \Gamma_{1,3}^{1111}(q_i=0) = u_{0R}, \quad \Gamma_{1,3}^{1122}(q_i=0) = u_{1R}, \quad \Gamma_{1,3}^{1133}(q_i=0) = u_{2R}, \\ &\frac{\partial}{\partial(i\omega)} \Gamma_{1,1}^{11}(-q;q)\Big|_{q=0} = 1, \quad \frac{\partial}{\partial(\boldsymbol{q}_\perp{}^2)} \Gamma_{1,1}^{11}(-q;q)\Big|_{q=0} = D_R, \quad \frac{\partial}{\partial(q_\parallel^2)} \Gamma_{1,1}^{11}(-q;q)\Big|_{q=0} = \rho_R, \\ &\frac{\partial}{\partial(ik_\parallel)} \Gamma_{1,2}^{123}\left(-k; \frac{k}{2}, \frac{k}{2}\right)\Big|_{k=0} = e_{pR}, \quad \frac{\partial}{\partial(ik_\parallel)} \Gamma_{1,2}^{123}\left(0; -\frac{k}{2}, \frac{k}{2}\right)\Big|_{k=0} = e_{mR}, \end{aligned} \quad (30)$$

where the momentum conservation for each vertex functions has already been taken into account (so no delta functions are multiplied). Employing the dimensional regularization with minimal subtraction scheme [17] along with the normalization conditions above, we obtain the renormalization factors to one-loop order (see Appendix for the details) as follows:

$$\begin{aligned} &Z = 1 + \frac{v_m^2}{4\epsilon}, \quad Z_D = 1 + \frac{v_m^2}{6\epsilon}, \quad Z_T = 1 - \frac{v_m^2}{2\epsilon}, \quad Z_\rho = 1 + \frac{3}{4\epsilon}(v_m^2 - v_p^2), \\ &Z_r = 1 + \frac{1}{2\epsilon}(g_0 + g_1 + g_2 + 2v_m^2), \quad Z_p = 1 + \frac{1}{8\epsilon}\left(7(g_1+g_2) - 3v_m^2 - 2\frac{v_m}{v_p}(g_1 - g_2)\right), \\ &Z_e = 1 + \frac{1}{8\epsilon}\left(3v_m^2 + 2v_p^2 + 3\frac{v_p}{v_m}(g_1 - g_2)\right), \quad Z_0 = 1 + \frac{3g_0}{2\epsilon} + \frac{3g_1 g_2}{\epsilon g_0} + \frac{3v_m^2}{4\epsilon g_0}(g_1 + g_2 - 2v_m^2 + 2v_p^2), \end{aligned} \quad (31)$$

$$Z_1 = 1 + \frac{g_2^2}{2g_1\epsilon} + \frac{v_m^2}{4g_1\epsilon}\big[g_0 + g_1 - 2\big(g_2 + v_m^2\big)\big] + \frac{1}{\epsilon}(g_0 + g_1 + g_2) + \frac{v_m v_p}{4g_1\epsilon}[g_1 + g_2 + v_m(3v_m - v_p)],$$

$$Z_2 = 1 + \frac{g_1^2}{2g_2\epsilon} + \frac{v_m^2}{4g_2\epsilon}\big[g_0 + g_2 - 2\big(g_1 + v_m^2\big)\big] + \frac{1}{\epsilon}(g_0 + g_1 + g_2) - \frac{v_m v_p}{4g_2\epsilon}[g_1 + g_2 + v_m(3v_m + v_p)],$$

where $\epsilon = 4 - d$; and the dimensionless expansion parameters

$$g_i = \frac{A_d T}{D^2\sqrt{\rho}} u_i \mu^{-\epsilon}, \quad v_s = \left(\frac{A_d T}{D^3\rho^{3/2}}\right)^{1/2} e_s \mu^{-\epsilon/2}, \tag{32}$$

where $i = 0$, 1, or 2, and s is either p or m; and the convenient geometric factor $A_d = 2\Gamma(3 - d/2)/(4\pi)^{d/2}$, where Γ here is the Euler gamma function. Furthermore, we obtain the following RG flow equations to one-loop order:

$$\mu\frac{dg_0}{d\mu} = -g_0\epsilon + \frac{3}{8}g_0\big(4g_0 + v_p^2\big) + 3g_1g_2 + \frac{v_m^2}{8}\big[6(g_1 + g_2) - 11g_0 + 12v_p^2 - 12v_m^2\big], \tag{33}$$

$$\mu\frac{dg_1}{d\mu} = g_1(-\epsilon + g_0 + g_1 + g_2) + \frac{g_2^2}{2} + \frac{v_p^2}{8}\big(3g_1 - 2v_m^2\big) + \frac{v_m v_p}{4}\big(g_1 + g_2 + 3v_m^2\big) + \frac{v_m^2}{8}\big(2g_0 - 9g_1 - 4g_2 - 4v_m^2\big), \tag{34}$$

$$\mu\frac{dg_2}{d\mu} = g_2(-\epsilon + g_0 + g_2 + g_1) + \frac{g_1^2}{2} + \frac{v_p^2}{8}\big(3g_2 - 2v_m^2\big) - \frac{v_m v_p}{4}\big(g_2 + g_1 + 3v_m^2\big) + \frac{v_m^2}{8}\big(2g_0 - 9g_2 - 4g_1 - 4v_m^2\big), \tag{35}$$

$$\mu\frac{dv_p}{d\mu} = \frac{v_p}{16}\big[-8\epsilon + 14(g_1 + g_2) - 22v_m^2 + 9v_p^2\big] - \frac{v_m}{4}(g_1 - g_2), \tag{36}$$

$$\mu\frac{dv_m}{d\mu} = \frac{v_m}{16}\big(-8\epsilon + 13v_p^2 - 10v_m^2\big) + \frac{3}{8}v_p(g_1 - g_2). \tag{37}$$

We solve for the RG fixed points numerically and find 72 fixed-point solutions. Out of these, 56 solutions are complex valued and, hence, being unphysical, are discarded, while the rest of the fixed points are discussed below. We denote a fixed point as $(g_0^*, g_1^*, g_2^*, v_p^*, v_m^*)$. After identifying the fixed points, we analyze the linearized flow equations to find their (local) stability.

There are four equilibrium fixed points for which the bias couplings vanish, $v_p^* = v_m^* = 0$, and the other couplings are as follows:

$$\text{Gaussian}: g_0^* = g_1^* = g_2^* = 0, \tag{38a}$$

$$\text{Ising}: g_0^* = \tfrac{2}{3}\epsilon, \quad g_1^* = g_2^* = 0, \tag{38b}$$

$$\text{Cubic}: g_0^* = \tfrac{4}{9}\epsilon, \quad g_1^* = g_2^* = \tfrac{2}{9}\epsilon, \tag{38c}$$

$$\text{Heisenberg}: g_0^* = \tfrac{6}{11}\epsilon, \quad g_1^* = g_2^* = \tfrac{2}{11}\epsilon. \tag{38d}$$

In the absence of spatial-anisotropic perturbations, the Heisenberg fixed point is stable for $\epsilon > 0$ (i.e., $d < 4$), while the Gaussian fixed point is stable for $d > 4$. Note that, even if the system has only the cyclic-permutation symmetry, the full permutation symmetry is restored asymptotically.

In addition to those listed in (38), we find the following fixed points that also respect the full permutation-symmetric theory (namely, $v_m = 0$ and $g_1 = g_2$):

$$\text{P}_\text{G}: g_0^* = g_1^* = 0, \quad E_p^* = \tfrac{8}{9}\epsilon, \tag{39a}$$

$$\text{P}_\text{I}: g_0^* = \tfrac{4}{9}\epsilon, \quad g_1^* = 0, \quad E_p^* = \tfrac{8}{9}\epsilon, \tag{39b}$$

$$\text{P}_\text{C}: g_0^* = \tfrac{2}{5}\epsilon, \quad g_1^* = \tfrac{1}{5}\epsilon, \quad E_p^* = \tfrac{4}{15}\epsilon, \tag{39c}$$

$$\text{P}_\text{H}: g_0^* = \tfrac{6}{13}\epsilon, \quad g_1^* = \tfrac{2}{13}\epsilon, \quad E_p^* = \tfrac{16}{39}\epsilon, \tag{39d}$$

where $E_p \equiv v_p^2$. The fixed points are so labeled because of the structural similarity with the corresponding points in Eq. (38). Here, we do not distinguish between v_p^* and $-v_p^*$, since choosing one of them amounts to choosing the bias direction. More precisely, changing the sign of bias parameters $\{v_p, v_m\} \to \{-v_p, -v_m\}$ will not take us to a new fixed point with different critical exponents.

When all the couplings are tuned off except e_p, RG flows only along the line $g_0 = g_1 = g_2 = v_m = 0$. In this case, there are two fixed points, Gaussian and P_G, and the fixed point P_G is stable (unstable) if $\epsilon > 0$ ($\epsilon < 0$). To our knowledge, this fixed point was not known before in the literature. In the one-component case $N = 1$, a similar stable fixed point is found by Hwa and Kardar [21].

For the choice $u_1 = u_2 = e_m = 0$ in Eq. (17), the one-loop calculations show that there are four fixed points (Gaussian, Ising, P_G, and P_I), where P_I is the only stable fixed point for $\epsilon > 0$. Although the linear stability analysis alludes to the existence of a universality class in the (g_0, E_p) subspace, the higher-order loop corrections rule out this possibility. For instance, adding a $\widetilde{\phi}_1\phi_1^3$ vertex to Fig. 6(c), with $a = 1$, $b = c = c_2 = c_3 = 2$, and $c_1 = 3$, generates g_1 at two-loop order, and, hence, the RG flow pushes the system out of the (g_0, E_p) subspace.

Thus, in the space of all perturbations that preserve the full permutation symmetry ($u_1 = u_2$ and $e_m = 0$), there are

eight fixed points, among which only one is stable; P_H is stable for $\epsilon > 0$ ($d < 4$), while the Gaussian is stable for $\epsilon < 0$ ($d > 4$). Hence, unlike the $N = 1$ case, the bias perturbations in the $N = 3$ case are highly relevant and can lead to a new universality class.

Let us now also include the v_m term, which breaks the permutation symmetry to cyclic-permutation symmetry. Suppose we first restrict to a subspace with the choice $v_p = 0$ and $g_1 = g_2$, then the action (17) is invariant under the transformation $\phi_1 \leftrightarrow \phi_2$ and $e_m \to -e_m$, and hence the symmetry constrains the RG flow to the $(g_0, g_1 = g_2, v_m)$ subspace. For $\epsilon > 0$, the fixed points are the equilibrium ones with $v_m^* = 0$. This special case was studied earlier in Ref. [11], where, in contrast to our result, a stable fixed point was found. However, in Ref. [11], it was numerically observed that the system exhibits chaotic behavior in the noiseless (zero-temperature) limit. We argue that this numerical observation is more consistent with our result than the existence of a stable fixed point. The absence of a stable fixed point signifies that there is no order-disorder phase transition. Since the system in the infinite-temperature limit should be fully disordered and in the zero-temperature limit, the behavior is also chaotic, there is no ordered phase in the system (assuming there is, at most, one transition). We thus expect that there is no phase transition, or in other words, no stable fixed point, as confirmed by our analysis.

If we do not restrict the study to the $(g_0, g_1 = g_2, v_m)$ subspace and instead explore the space of all coupling constants, we then obtain the following fixed point:

$$g_0^* = 1.49763\epsilon, \quad g_1^* = -1.86313\epsilon, \quad g_2^* = 1.12359\epsilon, \\ v_p^* = 2.02811\sqrt{\epsilon}, \quad v_m^* = 1.06466\sqrt{\epsilon}, \tag{40}$$

which is unstable, and also find three other unstable fixed points. The other unstable fixed points can be obtained from the above by taking $\{v_p^*, v_m^*\} \to \{-v_p^*, -v_m^*\}$ and $\{g_1^*, g_2^*, v_p^*\} \to \{g_2^*, g_1^*, -v_p^*\}$ or $\{g_1^*, g_2^*, v_m^*\} \to \{g_2^*, g_1^*, -v_m^*\}$. Note that the flow equations are invariant under these transformations.

The fixed-point analysis tells us that the presence of the e_m term will destabilize the $N = 3$ field theories.

IV. SUMMARY

To sum up, we have studied the effect of spatially anisotropic perturbations on nonconserved N-vector models.

We first constructed spatially anisotropic N-vector models that obey Langevin dynamics, and contain the most general marginal interactions at $d = 4$. If the dynamics is invariant under all the permutations of the field components, then the number of coupling constants can be at most 12 (7 ϕ^4-type G couplings and 5 bias $\mathcal{E}$ couplings). We then argued that single-length-scale field theories with bias are possible only for $N = 1$ or certain $N = 3$ models. The $N = 1$ (BS) theory has been studied earlier [7], where the bias was found to be marginally irrelevant. For $N = 2$ or $N > 3$, we see that the bias generates off-diagonal mass terms and rules out the possibility of Langevin field theories with a single length scale. Hence, the $N = 2$ models and the generic $N > 3$ models, when subjected to bias, should behave like the BS model [7] in the large-distance limit. We also confirmed this by analyzing numerically an $N = 2$ model with bias.

For $N = 3$ field theories with a single length scale, the full permutation symmetry allows only one kind of bias coupling (labeled e_p), while the cyclic-permutation symmetry allows another additional coupling (labeled e_m). We followed the renormalization-group flows, up to one-loop order, for the $N = 3$ systems that are invariant under cyclic permutations of the field components. In this case, the coupling-constant space is five dimensional, with three ϕ^4-type couplings (u_0, u_1, u_2) and two bias couplings (e_p and e_m); see Eq. (17). We find that, in the presence of e_m perturbations, no stable fixed point exists.

Once the e_m term is thrown away (and $u_1 = u_2$ is set), the system becomes permutation symmetric and has eight fixed points as given in Eqs. (38) and (39). Only two of the fixed points are stable: the fixed point P_H [see Eq. (39d)] is stable for $\epsilon > 0$ ($d < 4$), while the Gaussian fixed point is stable for $\epsilon < 0$ ($d > 4$). Hence, we find a new universality class governed by the fixed point P_H for $N = 3$ systems with a spatial-anisotropic bias.

We also find another universality class when all the coupling constants except e_p are tuned off. In this case, the RG flow does not generate other couplings and leads to a nontrivial stable fixed point, denoted P_G [see Eq. (39a)].

In general, nonconserved N-vector models are sensitive to spatial-anisotropic perturbations, and the large-distance properties are governed by the kinetic Ising class, except for $N = 3$. In the case of $N = 3$, we found two universality classes governed by P_G and P_H.

ACKNOWLEDGMENTS

S.D. acknowledges the generous support by the people of South Korea, and the Korea Institute for Advanced Study, where the work was initiated. S.-C. P. would like to acknowledge the support by DFG within SFB 680 *Molecular Basis of Evolutionary Innovations*; the support by the Catholic University of Korea, Research Fund, 2010: and the support by the Basic Science Research Program through the National Research Foundation of Korea (NRF) funded by the Ministry of Education, Science and Technology (Grant No. 2010-0006306)

APPENDIX: ONE-LOOP CALCULATIONS

1. Integrals in dimensional regularization

The list of integrals required for dimensional regularization [17] are

$$\int \frac{d^d \boldsymbol{p}}{(2\pi)^d} (\boldsymbol{p}_\perp^2 + \rho p_\parallel^2 + r)^{-2} = \frac{A_d r^{-\epsilon/2}}{\epsilon \rho^{1/2}}, \tag{A1}$$

$$\int \frac{d^d \boldsymbol{p}}{(2\pi)^d} p_\parallel^2 (\boldsymbol{p}_\perp^2 + \rho p_\parallel^2 + r)^{-3} = \frac{A_d r^{-\epsilon/2}}{4\epsilon \rho^{3/2}}, \tag{A2}$$

$$\int \frac{d^d \boldsymbol{p}}{(2\pi)^d} p_\parallel^4 (\boldsymbol{p}_\perp^2 + \rho p_\parallel^2 + r)^{-4} = \frac{A_d r^{-\epsilon/2}}{8\epsilon \rho^{5/2}}, \tag{A3}$$

$$\int \frac{d^d \boldsymbol{p}}{(2\pi)^d} p_2^2 p_\parallel^2 (\boldsymbol{p}_\perp^2 + \rho p_\parallel^2 + r)^{-4} = \frac{A_d r^{-\epsilon/2}}{24\epsilon \rho^{3/2}}, \tag{A4}$$

where p_2 in the last equation (A4) stands for one of the perpendicular components of $\boldsymbol{p}$ and $A_d \equiv 2\Gamma(3 - d/2)/(4\pi)^{d/2}$ is a geometric factor.

2. Diagrammatics

Let V_i denote the number of i-legged vertices (see. Fig. 2) in the loop expansion for $\Gamma_{\tilde{m},m}$, and let $V = V_2 + V_3 + V_4$ denote the total number of vertices in a diagram. Since the number of φ fields in the internal integration should be equal to that of $\tilde{\varphi}$, the number of internal lines I is given by

$$I \equiv 2V_2 + V_3 + V_4 - \tilde{m} = 2V_3 + 3V_4 - m. \tag{A5}$$

If there are L number of loops, then the relation $I - V = L - 1$ should hold, and it therefore follows that

$$V_2 = \tilde{m} + L - 1, \quad V_3 + 2V_4 = m + \tilde{m} + 2(L-1), \tag{A6}$$

which, in the case of one-loop calculations, reduce to

$$V_2 = \tilde{m}, \quad V_3 + 2V_4 = m + \tilde{m}. \tag{A7}$$

For notational convenience, we define the following function that is associated to momentum-dependent 3-legged vertices:

$$\lambda(q_1,q_2,q_3) = ie_p q_{1\parallel} + ie_m(q_{2\parallel} - q_{3\parallel}), \tag{A8}$$

and the correlation function

$$C_0(p) = G_0(p)G_0(-p). \tag{A9}$$

3. $\Gamma^{aa}_{1,1}(-q;q)$

The solutions of Eq. (A7) for $\tilde{m} = m = 1$ are (a) $V_3 = 0$ and $V_4 = 1$ and (b) $V_3 = 2$ and $V_4 = 0$. The corresponding one-particle irreducible (1PI) diagrams are illustrated in Fig. 3. Note that none of the diagrams in Fig. 3 can generate off-diagonal mass terms, as expected from our general arguments. The loop integrals for Fig. 3 are

$$\text{(a)} = T(u+u_1+u_2)\int_p C_0(p) = -Dr\frac{u+u_1+u_2}{2}B_\epsilon, \tag{A10}$$

$$\begin{aligned}\text{(b)} &= -2T\int_p G_0(p-q)C_0(p)[\lambda(q,p-q,-p)\lambda(-p+q,p,-q) + \lambda(q,-p,p-q)\lambda(-p+q,-q,p)] \\ &= -\left(i\omega e_m^2 + D\boldsymbol{q}_\perp^2\frac{e_m^2}{6} + D\rho q_\parallel^2\frac{3}{4}\left(e_m^2 - e_p^2\right) + Dre_m^2\right)C_\epsilon + \cdots,\end{aligned} \tag{A11}$$

where

$$B_\epsilon = \frac{A_d T}{D^2\sqrt{\rho}\epsilon}r^{-\epsilon/2}, \quad C_\epsilon = \frac{A_d T}{D^3\rho^{3/2}\epsilon}r^{-\epsilon/2}, \tag{A12}$$

and the ellipsis contains the finite parts that shall be dropped in the minimal-subtraction (MS) scheme that we adopt. In the remainder, the integrals are evaluated in the MS scheme.

4. $\Gamma^{11}_{2,0}(-q,q)$

There are two solutions for Eq. (A7) with $m = 0$ and $\tilde{m} = 2$: $\{V_3 = 2, V_4 = 0\}$ and $\{V_3 = 0, V_4 = 1\}$. However, the latter solution does not yield any 1PI diagram. Hence, there is only one diagram that is depicted in Fig. 4. The one-loop correction to $\Gamma^{11}_{2,0}(-q,q)$ is

$$-4T^2\int_p C_0(p)^2|\lambda(0,p,-p)|^2 = -Te_m^2C_\epsilon. \tag{A13}$$

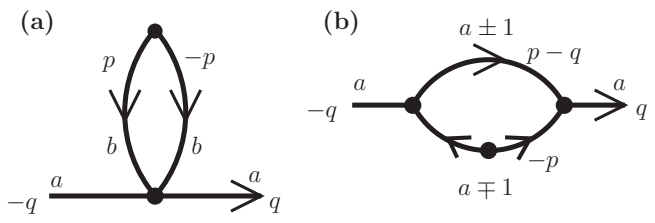

FIG. 3. One-loop diagrams for $\Gamma^{aa}_{1,1}(-q;q)$. The internal momentum which should be integrated out is denoted by p. The value of b can be 1, 2, or 3.

5. $\Gamma^{123}_{1,2}(q_1;q_2,q_3)$

When $\tilde{m} = 1$ and $m = 2$, there are two solutions for Eq. (A7): $\{V_3 = 1, V_4 = 1\}$ or $\{V_3 = 3, V_4 = 0\}$. For each set of solutions, two different 1PI diagrams can be drawn. For $V_2 = V_3 = V_4 = 1$, the diagrams are given in Figs. 5(a) and 5(b), while the diagrams for the other solution are given in Figs. 5(c) and 5(d). We now calculate these diagrams one by one.

For Fig. 5(a), depending on the values of $\{b,c,a_1,a_2\}$, four different combinations are possible: (a1) $b = 2$ and $c = 3$, and either $\{a_1 = 1, a_2 = 2\}$ or $\{a_1 = 2, a_2 = 1\}$; and (a2) $b = 3$ and $c = 2$, and either $\{a_1 = 1, a_2 = 3\}$ or $\{a_1 = 3, a_2 = 1\}$.

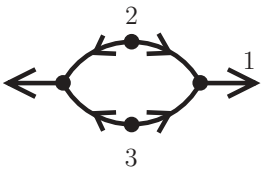

FIG. 4. One-loop diagram for $\Gamma^{11}_{2,0}(-q,q)$.

Let us define the following operation $\mathcal{O}$, which transforms the momenta and coupling constants of the diagram:

$$\mathcal{O} = \{q_2 \leftrightarrow q_3, \quad u_1 \leftrightarrow u_2, \quad e_m \rightarrow -e_m\}. \tag{A14}$$

Due to the cyclic symmetry, the result for (a2) can be readily achieved by operating $\mathcal{O}$ to (a1). Since

$$\text{(a1)} = -2Tu_1 \int_p G_0(p-q_3)C_0(p)[\lambda(-p+q_3,-q_3,p) + \lambda(-p+q_3,p,-q_3)] = -\frac{3}{4} i e_p q_{3\parallel} u_1 B_\epsilon, \tag{A15}$$

we get

$$\text{(a)} = \text{(a1)} + \text{(a2)} = -\frac{3}{4} i e_p B_\epsilon (q_{3\parallel} u_1 + q_{2\parallel} u_2). \tag{A16}$$

For Fig. 5(b), either $\{a_1 = 2,\ a_2 = 3\}$ or $\{a_1 = 3,\ a_2 = 2\}$ should be satisfied. Note that the interaction strength for $\tilde{\varphi}_2\varphi_2\varphi_3^2$ is u_1 and that for $\tilde{\varphi}_3\varphi_3\varphi_2^2$ is u_2. Hence, we get

$$\begin{aligned}\text{(b)} &= -2T \int_p G_0(p+q)C_0(p)[u_1\lambda(-q_1,p+q_1,-p) + u_2\lambda(-q_1,-p,p+q_1)] \\ &= -iq_{1\parallel}[(u_1-u_2)e_m - 2(u_1+u_2)e_p]\frac{B_\epsilon}{4}.\end{aligned} \tag{A17}$$

For Figs. 5(c) and 5(d), it is convenient to introduce

$$I_d(p;q_1,q_2) = C_0(p)G_0(p-q_2)G_0(p+q_1), \tag{A18}$$

$$I_e(p;q_2,q_3) = C_0(p)G_0(p-q_2)G_0(-p-q_3). \tag{A19}$$

It is easy to see that either $\{b = 2,\ c = 3\}$ or $\{b = 3,\ c = 2\}$ should be satisfied in Fig. 5(c). Thus,

$$\begin{aligned}\text{(c)} &= 2T \int_p I_d(p;q_1,q_3)\lambda(-q_1,-p,p+q_1)\lambda(-p-q_1,p-q_3,-q_2)\lambda(-p+q_3,p,-q_3) \\ &\quad + 2T \int_p I_d(p;q_1,q_2)\lambda(-q_1,p+q_1,-p)\lambda(-p-q_1,-q_3,p-q_2)\lambda(-p+q_2,-q_2,p) \\ &= -ie_p q_{1\parallel} C_\epsilon \frac{e_m^2 - e_p^2}{8} + ie_m q_{2\parallel} C_\epsilon \frac{(e_m-e_p)^2}{16} - ie_m q_{3\parallel} C_\epsilon \frac{(e_m+e_p)^2}{16}.\end{aligned} \tag{A20}$$

For Fig. 5(d), we get

$$\begin{aligned}\text{(d)} &= 2T \int_p I_e(p;q_2,q_3)\lambda(-q_1,-p-q_3,p-q_2)\lambda(-p+q_2,p,-q_2)\lambda(p+q_3,-q_3,-p) \\ &= -ie_p q_{1\parallel} C_\epsilon \frac{e_p^2 - e_m^2}{8} + ie_m q_{2\parallel} \frac{1}{16}(e_m+e_p)(5e_m+3e_p)C_\epsilon ie_m q_{3\parallel} \frac{1}{16}(e_m-e_p)(5e_m-3e_p)C_\epsilon.\end{aligned} \tag{A21}$$

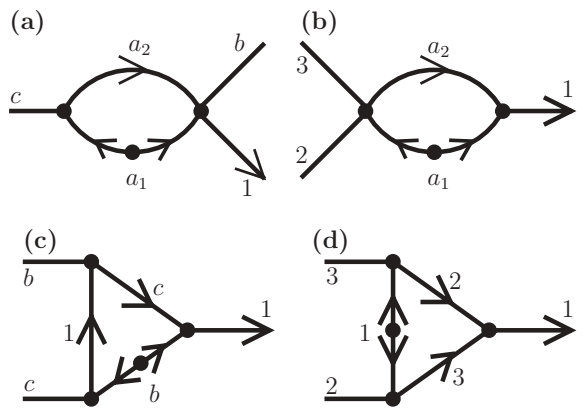

FIG. 5. One-loop diagrams for $\Gamma^{123}_{1,2}(q_1;q_2,q_3)$. For the external line with index i, set the momentum to $-q_i$ and use the momentum conservation at each vertex point. (a) If $a_1 = 1$ ($a_2 = 1$), then $a_2 = b$ ($a_1 = b$). Since b can be either 2 or 3, there are four different diagrams with this form. (b) Either $\{a_1 = 2,\ a_2 = 3\}$ or $\{a_1 = 3,\ a_2 = 2\}$. (c) Either $\{b = 2,\ c = 3\}$ or $\{b = 3,\ c = 2\}$. (d) There is a unique diagram.

6. $\Gamma^{1111}_{1,3}(q_1;q_2,q_3,q_4)$

For $\tilde{m} = 1$ and $m = 3$, there are three solutions for Eq. (A7): $\{V_3 = 0,\ V_4 = 2\}$, $\{V_3 = 2,\ V_4 = 1\}$, or $\{V_3 = 4,\ V_4 = 0\}$. There are eight different types of 1PI diagrams as shown in Fig. 6. Although the basic structure of diagrams is same for any $\Gamma_{1,3}$'s, the mathematical expression for $\Gamma^{1111}_{1,3}$ is different from $\Gamma^{1122}_{1,3}(q_1;q_2,q_3,q_4)$. Hence, we evaluate them separately; $\Gamma^{1111}_{1,3}$ is done in this section, while $\Gamma^{1122}_{1,3}$ is done in the next. Note that $\Gamma^{1133}_{1,3}$ can be found easily by applying $\mathcal{O}$ to $\Gamma^{1122}_{1,3}$. As a result of the normalization conditions, we will set $q_i = 0$ from now on.

The diagrams for $\Gamma^{1111}_{1,3}$ in Fig. 6 satisfy the condition $b = c = d = 1$. For the diagram in Fig. 6(a), a_1 should be equal to a_2, and can take the values 1, 2, or 3. Hence, the contribution from this diagram is

$$\begin{aligned}\text{(a)} &= -6T\left(u_0^2 + 2u_1u_2\right)\int_p G_0(p)C_0(p) \\ &= -\frac{3}{2}\left(u_0^2 + 2u_1u_2\right)B_\epsilon.\end{aligned} \tag{A22}$$

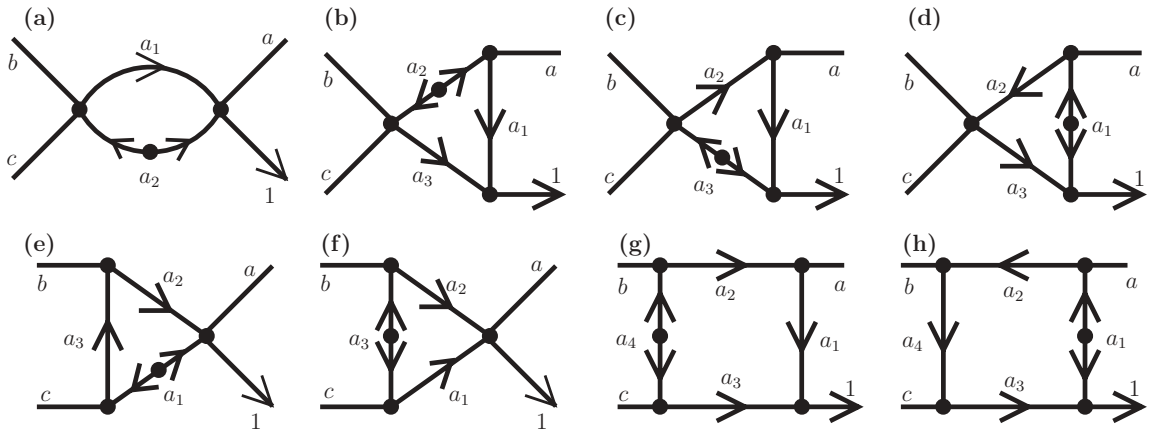

FIG. 6. One-loop diagrams for $\Gamma^{1abc}_{1,3}(q_1;q_2,q_3,q_4)$.

For Figs. 6(b), 6(c), and 6(d), either $\{a_1 = 2, a_2 = a_3 = 3\}$ or $\{a_1 = 3, a_2 = a_3 = 2\}$ should be satisfied. Hence,

$$\begin{aligned}\text{(b)} &= 6T\int_p [u_2\lambda(0,p,-p)\lambda(p,0,-p) \\ &\quad + u_1\lambda(0,-p,p)\lambda(p,-p,0)]I_{e0}(p) \\ &= -\frac{3}{4}e_m[(u_1+u_2)e_m + (u_2-u_1)e_p]C_\epsilon, \end{aligned} \tag{A23}$$

$$\begin{aligned}\text{(c)} &= 6T\int_p [u_2\lambda(0,p,-p)\lambda(p,0,-p) \\ &\quad + u_1\lambda(0,-p,p)\lambda(p,-p,0)]I_{d0}(p) = \frac{1}{2}\text{(b)}, \end{aligned} \tag{A24}$$

$$\begin{aligned}\text{(d)} &= 6T\int_p [u_2\lambda(0,p,-p)\lambda(-p,p,0) \\ &\quad + u_1\lambda(0,-p,p)\lambda(-p,0,p)]I_{d0}(p) \\ &= \frac{1}{2}\text{(b)} - \frac{3}{4}(u_1-u_2)e_m e_p C_\epsilon, \end{aligned} \tag{A25}$$

where $I_{e0}(p) = I_e(p;0,0)$ and $I_{d0}(p) = I_d(p;0,0)$.

For Figs. 6(e) and 6(f), either $\{a_3 = 2, a_2 = a_1 = 3\}$ or $\{a_3 = 3, a_2 = a_1 = 2\}$ should be satisfied. Hence,

$$\begin{aligned}\text{(e)} &= 12T\int_p [u_2\lambda(-p,p,0)\lambda(-p,0,p) \\ &\quad + u_1\lambda(-p,0,p)\lambda(-p,p,0)]I_{d0}(p) \\ &= \frac{3}{8}(u_1+u_2)\left(e_m^2 - e_p^2\right)C_\epsilon, \end{aligned} \tag{A26}$$

$$\begin{aligned}\text{(f)} &= 6T\int_p [u_2\lambda(p,0,-p)\lambda(-p,0,p) \\ &\quad + u_1\lambda(-p,p,0)\lambda(p,-p,0)]I_{e0}(p) \\ &= \frac{3}{8}\big[2(u_2-u_1)e_m e_p + (u_1+u_2)e_m^2 \\ &\quad + (u_1+u_2)e_p^2\big]C_\epsilon. \end{aligned} \tag{A27}$$

For Figs. 6(g) and 6(h), we introduce, for notational convenience,

$$I_f(p) \equiv G_0(p)^3 G_0(-p)^2, \quad I_g(p) \equiv G_0(p)^4 G_0(-p). \tag{A28}$$

The nonvanishing contribution occurs when either $\{a_1 = a_4 = 2, a_2 = a_3 = 3\}$ or $\{a_1 = a_4 = 3, a_2 = a_3 = 2\}$. Hence, we obtain

$$\begin{aligned}\text{(g)} &= -12T\int_p I_f(p)\lambda(-p,p,0)\lambda(-p,0,p) \\ &\quad [\lambda(p,0,-p)\lambda(0,p,-p) \\ &\quad + \lambda(p,-p,0)\lambda(0,-p,p)] \\ &= 9e_m^2\left(e_m^2 - e_p^2\right)D_\epsilon, \end{aligned} \tag{A29}$$

$$\begin{aligned}\text{(h)} &= -12T\int_p I_g(p)\lambda(-p,p,0)\lambda(-p,0,p) \\ &\quad \times[\lambda(-p,0,p)\lambda(0,-p,p) \\ &\quad + \lambda(-p,p,0)\lambda(0,p,-p)] = \frac{1}{3}\text{(g)}, \end{aligned} \tag{A30}$$

where $D_\epsilon = C_\epsilon/(8D\rho)$.

7. $\Gamma^{1122}_{1,3}(q_1;q_2,q_3,q_4)$

For Fig. 6(a), the loop integral is always $\int_p G_0(p)C_0(p)$. We therefore have to decide which interaction terms are involved in the diagrams. If $a = 1$ and $b = c = 2$, then a_1 equals to a_2 and can take any index. If $a = b = 2$ and $c = 1$, then either $\{a_1 = 1, a_2 = 2\}$ or $\{a_1 = 2, a_2 = 1\}$ should be satisfied. Hence,

$$\text{(a)} = -\left(u_1^2 + u_0u_1 + u_2u_1 + \frac{u_2^2}{2}\right)B_\epsilon. \tag{A31}$$

For Figs. 6(b), 6(c), and 6(d), either $\{a = 1$ and $b = c = 2\}$ or $\{c = 1$ and $a = b = 2\}$ is required. If $a = 1$ and $b = c = 2$, then either $\{a_1 = 2, a_2 = a_3 = 3\}$ or $\{a_1 = 3, a_2 = a_3 = 2\}$ should be satisfied. If $c = 1$ and $b = a = 2$, then it follows that $a_1 = 3$, $a_2 = 1$, and $a_3 = 2$. Hence,

$$\begin{aligned}\text{(b)} &= 2T\int_p I_{e0}(p)\{u_2\lambda(p,-p,0)[\lambda(0,-p,p) \\ &\quad + 2\lambda(0,p,-p)] + u_0\lambda(0,p,-p)\lambda(p,0,-p)\} \\ &= -\frac{1}{4}e_m[(u_0-u_2)e_m + (u_0+u_2)e_p]C_\epsilon, \end{aligned} \tag{A32}$$

$$\begin{aligned}(\mathrm{c}) &= 2T\int_p I_{d0}(p)[u_2\lambda(p,-p,0)\lambda(0,-p,p)\\ &\quad + 2u_1\lambda(p,-p,0)\lambda(0,p,-p)\\ &\quad + u_0\lambda(0,p,-p)\lambda(p,0,-p)]\\ &= -\frac{3}{8}e_m[(u_1+u_2)e_m+(u_2-u_1)e_p]C_\epsilon, \qquad \text{(A33)}\end{aligned}$$

$$\begin{aligned}(\mathrm{d}) &= 2T\int_p I_{d0}(p)\{u_2\lambda(-p,0,p)[\lambda(0,-p,p)\\ &\quad + 2\lambda(0,p,-p)] + u_0\lambda(0,p,-p)\lambda(-p,p,0)\}\\ &= -\frac{1}{8}e_m[(u_0-u_2)e_m-(u_0+u_2)e_p]C_\epsilon. \qquad \text{(A34)}\end{aligned}$$

For Fig. 6(e), there are three possible cases: $\{a=1,\ b=c=2\}$, $\{b=1,\ a=c=2\}$, or $\{c=1,\ a=b=2\}$. If $a=1$ and $b=c=2$, then either $\{a_1=a_2=1,\ a_3=3\}$ or $\{a_1=a_2=3,\ a_3=1\}$ should be satisfied. If $c=1$ and $b=a=2$, then it follows that $a_1=2$, $a_2=1$, and $a_3=3$. If $b=1$ and $c=a=2$, then it follows that $a_1=1$, $a_2=2$, and $a_3=3$. Hence, we obtain

$$\begin{aligned}(\mathrm{e}) &= 4T\int_p I_{d0}(p)\{\lambda(-p,0,p)[u_1\lambda(-p,0,p)\\ &\quad + u_2\lambda(-p,p,0)+u_0\lambda(-p,p,0)]\\ &\quad + u_1\lambda(-p,p,0)^2\} = \frac{3}{8}(u_1+u_2)\left(e_m^2-e_p^2\right)C_\epsilon.\end{aligned} \qquad \text{(A35)}$$

For Fig. 6(f), out of the three possible cases that appear in the case 6(e), $\{a=1,\ b=c=2\}$, $\{b=1,\ a=c=2\}$, and $\{c=1,\ a=b=2\}$, the last two cases are identical, and it is therefore sufficient to consider only two possibilities. In the case $\{a=1$ and $b=c=2\}$, either $\{a_1=a_2=1, a_3=3\}$ or $\{a_1=a_2=3, a_3=1\}$ should be satisfied. In the case $\{c=1$ and $b=a=2\}$, it follows that $a_1=2$, $a_2=1$, and $a_3=3$. We thus obtain

$$\begin{aligned}(\mathrm{f}) &= 2T\int_p I_{e0}(p)\{\lambda(-p,0,p)[2u_1\lambda(p,-p,0)\\ &\quad + u_0\lambda(p,0,-p)] + \lambda(p,-p,0)\lambda(-p,p,0)\}\\ &= \frac{1}{8}\left[2(u_0-u_2)e_me_p+(u_0-2u_1+u_2)e_m^2\right.\\ &\quad \left.+(u_0+2u_1+u_2)e_p^2\right]C_\epsilon. \qquad \text{(A36)}\end{aligned}$$

Both Figs. 6(g) and 6(h), we have two possibilities: either $\{a=a_4=1,\ b=c=a_1=2,\ a_2=a_3=3\}$ or $\{a=b=a_3=2, c=a_2=1, a_1=a_4=3\}$. Hence, we obtain

$$\begin{aligned}(\mathrm{g}) &= -4T\int_p I_f(p)\lambda(-p,p,0)\lambda(p,-p,0)[\lambda(0,p,-p)\\ &\quad \times\lambda(-p,p,0)+\lambda(0,-p,p)\lambda(-p,0,p)]\\ &= 3e_m^2(e_m-e_p)^2D_\epsilon, \qquad \text{(A37)}\end{aligned}$$

$$\begin{aligned}(\mathrm{h}) &= -4T\int_p I_g(p)\lambda(-p,p,0)\lambda(-p,0,p)[\lambda(0,p,-p)\\ &\quad \times\lambda(-p,p,0)+\lambda(0,-p,p)\lambda(-p,0,p)]\\ &= e_m^2\left(e_m^2-e_p^2\right)D_\epsilon. \qquad \text{(A38)}\end{aligned}$$

[1] J. Marro and R. Dickman, *Nonequilibrium Phase Transitions in Lattice Models* (Cambridge University Press, Cambridge, 1999).
[2] A.-L. Barabasi and H. E. Stanley, *Fractal Concepts in Surface Growth* (Cambridge University Press, Cambridge, 1995).
[3] P. Bak, *How Nature Works: The Science of Self-Organized Criticality* (Springer, Berlin, 1996).
[4] B. Schmittmann and R. K. P. Zia, in *Phase Transitions and Critical Phenomena*, edited by C. Domb and J. L. Lebowitz (Academic, London, 1995), Vol. 17.
[5] P. C. Hohenberg and B. I. Halperin, Rev. Mod. Phys. **49**, 435 (1977).
[6] G. Grinstein, C. Jayaprakash, and Y. He, Phys. Rev. Lett. **55**, 2527 (1985).
[7] K. E. Bassler and B. Schmittmann, Phys. Rev. Lett. **73**, 3343 (1994).
[8] U. C. Täuber, V. K. Akkineni, and J. E. Santos, Phys. Rev. Lett. **88**, 045702 (2002).
[9] V. K. Akkineni and U. C. Täuber, Phys. Rev. E **69**, 036113 (2004).
[10] U. C. Täuber and E. Frey, Europhys. Lett. **59**, 655 (2002).
[11] J. Das, M. Rao, and S. Ramaswamy, Europhys. Lett. **60**, 418 (2002).
[12] K. E. Bassler and Z. Rácz, Phys. Rev. E **52**, R9 (1995).
[13] F. Haake, M. Lewenstein, and M. Wilkens, Z. Phys. B **55**, 211 (1984).
[14] See, e.g., p 640 of Géza Ódor, Rev. Mod. Phys. **76**, 663 (2004).
[15] P. C. Martin, E. D. Siggia, and H. H. Rose, Phys. Rev. A **8**, 423 (1973).
[16] E. Brézin, J. C. Le Guillou, and J. Zinn-Justin, Phys. Rev. B **10**, 892 (1974).
[17] D. J. Amit, *Field Theory, the Renormalization Group, and Critical Phenomena*, 2nd ed. (World Scientific, Singapore, 1984).
[18] See, e.g., M. Plischke and B. Bergersen, *Equilibrium Statistical Physics*, 3rd ed. (World Scientific, Singapore, 2006).
[19] G. Kamieniarz and H. W. J. Blöte, J. Phys. A: Math. Gen. **26**, 201 (1993); W. Selke, Eur. Phys. J. B **51**, 223 (2006).
[20] N. D. Mermin and H. Wagner, Phys. Rev. Lett. **17**, 1133 (1966).
[21] T. Hwa and M. Kardar, Phys. Rev. Lett. **62**, 1813 (1989).